Frequency-dependent rupture process of the 2011 M_w 9.0 Tohoku Earthquake: Comparison of short-period *P* wave backprojection images and broadband seismic rupture models

Keith D. Koper[1], Alexander R. Hutko[2], Thorne Lay[3], Charles J. Ammon[4], and Hiroo Kanamori[5]

[1]*Department of Geology and Geophysics, University of Utah, Salt Lake City, Utah 84112, USA*
[2]*Incorporated Research Institutions for Seismology, Data Management Center, Seattle, Washington 98105, USA*
[3]*Department of Earth and Planetary Sciences, University of California Santa Cruz, Santa Cruz, California 95064, USA*
[4]*Department of Geosciences, The Pennsylvania State University, University Park, Pennsylvania 16802, USA*
[5]*Seismological Laboratory, California Institute of Technology, Pasadena, California 91125, USA*

The frequency-dependent rupture process of the 11 March 2011 M_w 9.0 off the Pacific coast of Tohoku Earthquake is examined using backprojection (BP) imaging with teleseismic short-period (∼1 s) *P* waves, and finite faulting models (FFMs) of the seismic moment and slip distributions inverted from broadband (>3 s) teleseismic *P* waves, Rayleigh waves and regional continuous GPS ground motions. Robust features of the BPs are initial down-dip propagation of the short-period energy source with a slow rupture speed (∼1 km/s), followed by faster (2–3 km/s) rupture that progresses southwestward beneath the Honshu coastline. The FFMs indicate initial slow down-dip expansion of the rupture followed by concentrated long-period radiation up-dip of the hypocenter, then southwestward expansion of the rupture. We explore whether these differences correspond to real variations in energy release over the fault plane or represent uncertainties in the respective approaches. Tests of the BP results involve (1) comparisons with backprojection of synthetic *P* waves generated for the FFMs, and (2) comparisons of backprojection locations for aftershocks with corresponding NEIC and JMA locations. The data indicate that the down-dip environment radiates higher relative levels of short-period radiation than the up-dip regime for this great earthquake, consistent with large-scale segmentation of the frictional properties of the megathrust.

Key words: Great earthquakes, back-projection, reverse-time imaging, seismic energy.

1. Introduction

The 11 March 2011 off the Pacific coast of Tohoku (M_w 9.0) Earthquake ruptured the megathrust fault along which the Pacific plate underthrusts Honshu. Large earthquakes with $M_w \sim 7.2$–7.9 are relatively common along the down-dip portion of the megathrust seaward of Miyagi prefecture (e.g., Kanamori *et al.*, 2006; Umino *et al.*, 2006; Kimura *et al.*, 2010). This region is also recognized to have had a large tsunamigenic earthquake in 869 with a source area estimated to be further off-shore (Minoura *et al.*, 2001). Since that time, no regional earthquake has produced as large a tsunami; however, to the north, large tsunamis struck the northeastern coast of Honshu in 1611, 1896 and 1933, with wave run-up as high as 25 m (Iida *et al.*, 1967). The 1896 Meiji Sanriku earthquake was characterized as a tsunami earthquake by Kanamori (1972) and appears to have had slow rupture velocity with relatively low levels of short-period energy release but large displacements close to the trench. The 1933 Sanriku-oki earthquake was an outer rise event within the Pacific plate that

exhibited normal faulting and relatively high-stress-drop (Kanamori, 1971). The up-dip region of the megathrust off northeastern Honshu has small earthquakes with lower frequency characteristics than the down-dip and outer rise regions (Fukao and Kanjo, 1980). Over the past decade, GPS measurements have indicated significant strain accumulation along the Honshu megathrust (e.g., Mazzotti *et al.*, 2000; Nishimura *et al.*, 2004; Hashimoto *et al.*, 2009), but the seaward extent of strong strain accumulation was uncertain. This history suggests the possibility that the down-dip portion of the megathrust has different frictional properties than the up-dip portion; this can be evaluated using the seismic radiation from the great 2011 rupture.

The 2011 Tohoku Earthquake clearly differs from the 1896 earthquake in that it produced strong ground shaking along the coastline as well as a large tsunami. So the overall process for the 2011 event is distinctive from tsunami earthquakes such as the 1992 Nicaragua (Kanamori and Kikuchi, 1993), 2006 Java (Ammon *et al.*, 2006), and 2010 Mentawai (Lay *et al.*, 2011a) events, all of which had only weak near-source short-period shaking. The rupture area for the 2011 event is immense, with a width far greater than known tsunami earthquakes, and it is plausible that the event ruptured the entire megathrust width from trench to down-dip limit of coupling, thereby spanning a much greater zone

than the 1896 event is thought to have ruptured. This suggests the possibility that the event is a compound rupture, combining failure of an up-dip region that ruptures similarly to the 1896 tsunami earthquake and a down-dip region that ruptures like the conventional Miyagi-oki large earthquakes.

2.　Comparison of Rupture Models From Long-period and Short-period Data

We combine two basic procedures to constrain the general locations of short-period energy release and long-period energy release, comparing the results. The short-period energy source region is constrained by back-projection of regional network observations of teleseismic *P* waves (e.g., Ishii *et al.*, 2005; Xu *et al.*, 2009). The long-period energy source region is inferred from finite-fault seismic moment and slip inversions using both regional continuous GPS observations and broadband teleseismic *P* waves and Rayleigh waves. We consider two finite-fault models for the rupture process of the great 2011 Tohoku Earthquake obtained by our own processing: a least-squares inversion of teleseismic broadband *P* waves and a least-squares local-search algorithm joint inversion of teleseismic *P* waves and short-arc Rayleigh wave (R_1) relative source time functions (RSTF), with three-component continuous GPS (c-GPS) ground motion time series (30 s sampling) from along the Honshu coastline. Prior applications of these methods for great earthquake ruptures have been described in Lay *et al.* (2010) and Ammon *et al.* (2006). Ammon *et al.* (2011) describe the specific data set and procedures applied for the joint $P + R_1$ RSTF + c-GPS inversion and Lay *et al.* (2011c) describe the *P* wave inversion procedure.

Figures 1(a, b) display the finite-fault slip models from the two seismic inversion procedures, indicating the estimated variation in displacement on the fault. The models differ in roughness, with the *P*-wave inversion (Fig. 1(a)) having shorter spatial scale features in the solution, while the joint inversion (Fig. 1(b)) is smoother, with better overall spatial constraint due to use of a much wider range of seismic wave slownesses (including the near-field seismic waves in the c-GPS signals). Both models impose similar constraints on the rupture, the fault strike is 202°, the dip is 12°, the hypocentral location at which the grid is positioned is the USGS location (38.322°N, 142.369°E, depth into rock 24.4 km), and the rupture expansion speed is constrained to less than 1.5 km/s out to a distance of 100 km from the hypocenter and 2.5 km/s beyond that. The rupture velocity constraints were based on extensive modeling of the respective data sets. The peak fault displacements are about 42 m in each case, but the *P*-wave derived model uses a layered structure while the combined model uses a half-space in the slip estimation. As a result, the reduction of *S*-wave velocity in the layered crustal model results in an increase in slip at shallow depths toward the trench absent in the joint model. Generally, the models place most of the displacement at depths shallower than the hypocenter, with significant slip extending toward the trench; these attributes are shared with several other early finite-fault inversions available online, and are consistent with analysis of tsunami signals at Pacific DART buoys (Lay *et al.*, 2011b).
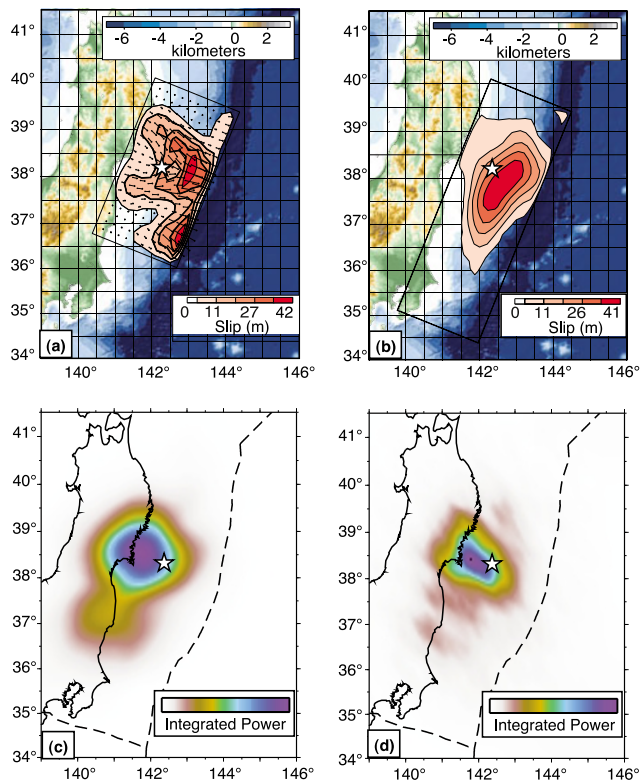

Fig. 1.　Seismically determined finite-fault rupture models for the 2011 Tohoku M_w 9.0 earthquake. The top panels show finite fault models developed using (a) broadband teleseismic *P*-waves and (b) teleseismic *P*, short-arc Rayleigh wave (R_1) relative source time functions, and continuous GPS recordings from Honshu. The bottom panels show time integrated beam power from backprojection of short period *P*-waves recorded over large station networks in (c) North America and (d) Europe. In each panel the white star indicates the USGS epicenter. The dashed lines in the lower panels show regional plate boundaries.

Two array configurations were used for backprojecting teleseismic *P* waves. The first consisted of 92 stations located in North America (NA) at distances of 71°–94° and azimuths of 21°–51° N. The stations were selected from a larger group to be evenly distributed in space and have *P* waves with a mean correlation coefficient of at least 0.85 as determined from a multi-channel cross correlation algorithm. The second array consisted of 119 stations located mainly in Europe (EU) at distances of 50°–93° and azimuths of 292°–355°, selected with similar considerations for high *P*-wave coherence and quasi-uniform geographical spacing. We experimented with denser array configurations and found little difference with the results presented below.

The backprojection technique of Xu *et al.* (2009) was applied to the data. The USGS hypocentral depth of 24.4 km was used with a grid spacing of 0.1°. Beam power was calculated from a 10-s long tapered window that was shifted in 1 s increments starting 20 s before the nominal USGS origin time and lasting for 220 s. Small perturbations to these processing parameters did not change the results.

We calculated beams using linear and fourth-root stacking. The former provides truer beam amplitudes, while the latter provides higher spatial resolution. We also experimented with two period ranges defined by 4-pole Butterworth bandpass filters with corners at 2 s and 0.5 s, and

10 s and 2 s. Time integrated maps of beam power from the fourth-root, short-period backprojections are presented in the bottom panels of Fig. 1. In contrast to the FFM slip models, most of the short-period energy projects to positions down-dip of the epicenter. This is also true of the linear short-period backprojections. The longer period backprojection images show a slight tendency for less down-dip energy and are arguably more similar to the FFM models, however the poorer resolution of the longer period band makes a direct comparison difficult. The basic pattern is slowly expanding short-period radiation from the down-dip region of the fault over about 80 s, followed by more rapid migration of the short-period source along the coastline for the next 80 s. The NA and EU array configurations produce similar results though they provide somewhat different resolution in the along-dip (better for NA) and along-strike (better for EU) directions, and the images correspond well with short-period backprojections produced by other groups.

3.   Test of Model Robustness

We assessed the robustness of the apparently frequency-dependent nature of the Tohoku rupture with two techniques. First, we backprojected synthetic *P*-waves calculated for the FFM shown in Fig. 1(a) using the same array configurations, processing steps, and control parameters as used for the data backprojections. If the synthetic images were to show significant down-dip energy, this would imply that the down-dip energy apparent in the data-derived images (Fig. 1(c, d)) is an artifact created by a wavefield interference effect that is not accounted for by our assumption of direct *P* backpropagation from receivers to source region.

We find that the images created from backprojecting the FFM synthetics have a substantially different pattern than those created from the short-period *P* wave data after an early stage of down-dip migration of source energy shared by both. For both the NA and EU array configurations, the synthetic images systematically show more energy to the east and up-dip of the energy on the data-derived images. This indicates that down-dip energy dominating the data backprojections is not an artifact of array geometry or Green function effects. We infer that the backprojection technique recovers the actual short-period source energy distribution in the form of beam power, and that this is associated with moderate or low seismic moment since it is not present in the finite fault model predictions.

In the second approach, we compared short-period backprojections from hours-long continuous processing for the NA and EU array configurations to source locations of more than 50 aftershocks located by the US Geological Survey and Japan Meteorological Agency (JMA). Most aftershocks are small enough to be considered point sources, so the time integrated beam power for these events is expected to locate close to the true epicenter. If these locations are substantially different than those determined from standard methods, it would indicate a bias in the backprojection technique caused by velocity anomalies along the general source-to-receiver array path.

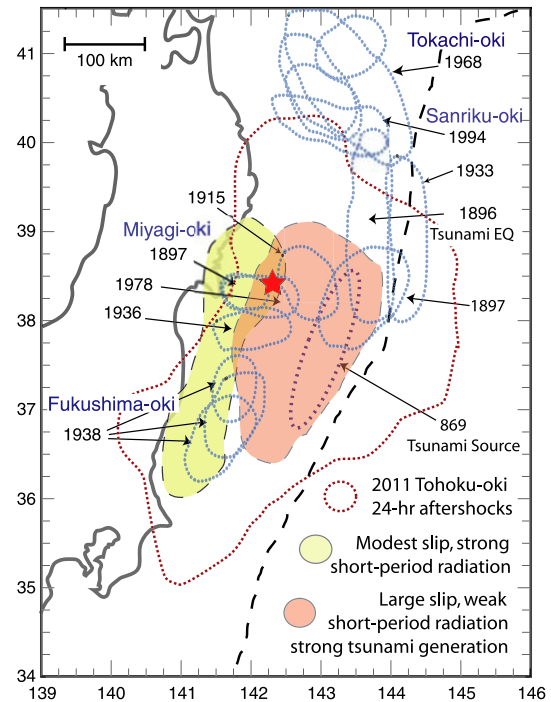We find that the back-projection locations are quite sim-

Fig. 2.   Summary schematic map of inferred fault zone rupture segmentation for the 11 March 2011 Tohoku Earthquake. The red star indicates the USGS location of the main event. The one-day aftershock region is indicated by red dots, extending ∼500 km along the subduction zone and includes outer rise activity off-shore of the region of large slip. The olive-colored region is where co-seismic short-period radiation with relatively low seismic moment is imaged by teleseismic *P*-waves. The orange-colored region is where little short-period radiation, but large slip is placed by broadband finite fault inversions of seismic and geodetic data. These are not precise areas, as both methods have uncertainties and limited resolution. Locations of historic offshore earthquake ruptures along the Tohoku coast are indicated with blue ellipsoidal shapes (Kanamori *et al.*, 2006). The approximate location of the 869 Jogan tsunami source region (Minoura *et al.*, 2001) is found to lie within the region of large slip. The magnitude ∼7.5 Miyagi-oki and Fukushima-oki earthquakes locate in the down-dip area. The 1896 tsunami earthquake appears to have ruptured similarly to the up-dip region in 2011, but the down-dip portion of the megathrust has not had recent large earthquakes and is also lacking in smaller event activity.

ilar to the catalog locations and show no systematic bias, with differences in location being comparable to discrepancies between the USGS and JMA locations. That this holds true for two arrays at distinct azimuths from the source region provides strong evidence that the down-dip location of mainshock short-period energy shown in the bottom panels of Fig. 1 is not an artifact created by velocity heterogeneity within the Earth or some imperfection in the reference model used in the analysis.

4.   Discussion and Conclusions

The great 2011 Tohoku event is one of the few well-recorded earthquakes with a large enough faulting distribution to explore spatial variations in frequency dependence of seismic radiation. Even so this is a difficult undertaking, as simplifying assumptions made in imaging and modeling procedures affect the inferred position of slip on the fault. No clear difference in long- vs. short-period radiation patterns has yet been discerned for the 2004 Sumatra (M_W 9.2) earthquake, but there is an indication that down-dip portions

of the 2010 Chile (M_w 8.8) rupture had strong short-period radiation (Kiser and Ishii, 2011), while longer-period radiation appears to have come from shallower positions on the megathrust (Lay *et al.*, 2010). The situation is arguably more convincing for the 2011 Tohoku Earthquake due to the very wide rupture area, the availability of multiple networks for back-projection imaging, and superb seismic and geodetic data sets.

Figure 2 summarizes the findings of our analysis; schematically, the megathrust appears to have depth-varying frictional properties that produce different seismic radiation during failure. We consider the down-dip region to produce conventional relative levels of short-period and long-period seismic waves, and this region has in fact experienced repeated large earthquake ruptures over the past century that were no larger than M_w 7.9. The up-dip region appears to fail with less short-period energy, perhaps related to slow rupture velocities, and for this event the primary slip of more than tens of meters occurred in the up-dip environment. The two FFMs indicate significant slip in the region of the 869 tsunami source, along the southward extension of the 1896 tsunami earthquake zone. If this portion of the fault plane is similar to that to the north, part of the 2011 rupture was effectively a tsunami earthquake while part of it was normal, faster rupture of the down-dip portion of the fault that typically fails in large $M_w \sim 7.5$ events.

Refined analysis of these first indications of frequency-dependent radiation from the megathrust is desirable. In particular, it is important to examine whether the strong motion data recorded across Japan is consistent with the deep, near coastal source of short-period energy proposed here and in other backprojection analyses of the giant Tohoku Earthquake of 2011. Early results indicate that this is the case; while longer period energy in the strong motion recordings originates from far off shore, higher frequency signal appears to predominantly come from the down-dip region of the megathrust (e.g., Ide *et al.*, 2011).

References

Ammon, C. J., H. Kanamori, T. Lay, and A. A. Velasco, The 17 July 2006 Java tsunami earthquake, *Geophys. Res. Lett.*, **233**, L234308, doi:10.10239/2006GL028005, 2006.

Ammon, C. J., T. Lay, H. Kanamori, and M. Cleveland, A rupture model of the 2011 off the Pacific coast of Tohoku Earthquake, *Earth Planets Space*, **63**, this issue, 693–696, 2011.

Fukao, Y. and K. Kanjo, A zone of the low-frequency earthquakes beneath the inner wall of the Japan trench, *Tectonophysics*, **67**, 153–162, 1980.

Hashimoto, C., A. Noda, T. Sagiya, and M. Matsu'ura, Interplate seismogenic zones along the Kuril-Japan trench inferred from GPS data inversion, *Nature Geosci.*, **2**, doi:10.1038/NGEO421, 2009.

Ide, S., A. Baltay, and G. C. Beroza, Shallow dynamic overshoot and energetic deep rupture in the 2011 M_w 9.0 Tohoku-Oki earthquake, *Science*, **332**, 1426–1429, 2011.

Iida, K., D. C. Cox, and G. Pararas-Carayannis, Preliminary catalog of tsunamis occurring in the Pacific Ocean, Data Rep. 5, HIG-67-10, Hawaii Inst. of Geophys. Univ. of Hawaii, Honolulu, pp. 261, 1967.

Ishii, M., P. M. Shearer, H. Houston, and J. E. Vidale, Extent, duration and speed of the 2004 Sumatra-Andaman earthquake imaged by the Hi-net array, *Nature*, **435**, 933–936, 2005.

Kanamori, H., Seismological evidence for a lithospheric normal faulting; the Sanriku earthquake of 1933, *Phys. Earth Planet. Inter.*, **4**, 289–300, 1971.

Kanamori, H., Mechanism of tsunami earthquakes, *Phys. Earth Planet. Inter.*, **6**, 346–359, 1972.

Kanamori, H. and M. Kikuchi, The 1992 Nicaragua earthquake: A slow tsunami earthquake associated with subducted sediments, *Nature*, **361**, 714–716, 1993.

Kanamori, H., M. Miyazawa, and J. Mori, Investigation of the earthquake sequence off Miyagi prefecture with historical seismograms, *Earth Planets Space*, **58**, 1533–1541, 2006.

Kimura, T., K. Koketsu, H. Miyake, C. Wu, and T. Miyatake, Dynamic source modeling of the 1978 and 2005 Miyagi-oki earthquakes: Interpretation of fracture energy, *J. Geophys. Res.*, **115**, B08302, doi:10.1029/2009JB006758, 2010.

Kiser, E. and M. Ishii, The 2010 Mw 8.8 Chile earthquake: Triggering on multiple segments and frequency-dependent rupture behavior, *Geophys. Res. Lett.*, **38**, L07301, doi:10.1029/2011GL047140, 2011.

Lay, T., C. J. Ammon, H. Kanamori, K. D. Koper, O. Sufri, and A. R. Hutko, Teleseismic inversion for rupture process of the 27 February 2010 Chile (Mw 8.8) earthquake, *Geophys. Res. Lett.*, **37**, L13301, doi:10.1029/2010GL043379, 2010.

Lay, T., C. J. Ammon, H. Kanamori, Y. Yamazaki, K. F. Cheung, and A. R. Hutko, The 25 October 2010 Mentawai tsunami earthquake (Mw 7.8) and the tsunami hazard presented by shallow megathrust ruptures, *Geophys. Res. Lett.*, **38**, L06302, doi:10.1029/2010GL046552, 2011a.

Lay, T., Y. Yamazaki, C. J. Ammon, K. F. Cheung, and H. Kanamori, The 2011 M_w 9.0 off the Pacific coast of Tohoku Earthquake: Comparison of deep-water tsunami signals with finite-fault rupture model predictions, *Earth Planets Space*, **63**, this issue, 797–801, 2011b.

Lay, T., C. J. Ammon, H. Kanamori, L. Xue, and M. J. Kim, Possible large near-trench slip during the 2011 M_w 9.0 off the Pacific coast of Tohoku Earthquake, *Earth Planets Space*, **63**, this issue, 687–692, 2011c.

Mazzotti, S., X. Le Pichon, P. Henry, and S. Miyazaki, Full interseismic locking of the Nankai and Japan-west Kurile subduction zones: An analysis of uniform elastic strain accumulation in Japan constrained by permanent GPS, *J. Geophys. Res.*, **105**, 13159–13177, 2000.

Minoura, K., F. Imamura, D. Sugawara, Y. Kono, and T. Iwashita, The 869 Jogan tsunami deposit and recurrence interval of large-scale tsunami on the Pacific coast of northeast Japan, *J. Nat. Disaster Sci.*, **23**(2), 83–88, 2001.

Nishimura, T., T. Hirasawa, S. Miyazaki, T. Sagiya, T. Tada, S. Miura, and K. Tanaka, Temporal change of interplate coupling in northeastern Japan during 1995–2002 estimated from continuous GPS observations, *Geophys. J. Int.*, **157**, 901–916, 2004.

Umino, N., T. Kono, T. Okada, J. Nakajima, T. Matsuzawa, N. Uchida, A. Hasegawa, Y. Tamura, and G. Aoki, Revisiting the three M=7.4 Miyagioki earthquakes in the 1930s: Possible seismogenic slip on asperities that were re-ruptured during the 1978 M=7.4 Miyagi-oki earthquake, *Earth Planets Space*, **58**, 1587–1592, 2006.

Xu, Y., K. D. Koper, O. Sufri, L. Zhu, and A. R. Hutko, Rupture imaging of the Mw 7.9 12 May 2008 Wenchuan earthquake from back projection of teleseismic P waves, *Geochem. Geophys. Geosyst.*, **10**, Q04006, doi:10.1029/2008GC002335, 2009.

K. D. Koper (e-mail: koper@seis.utah.edu), A. R. Hutko, T. Lay, C. J. Ammon, and H. Kanamori